Hot Electron Field Emission *via* Individually Transistor-Ballasted Carbon Nanotube Arrays

Chi Li,[†,‡,#] Yan Zhang,[†,#,*] Matthew T. Cole,[†,#,*] Sai G. Shivareddy,[†] Jon S. Barnard,[§] Wei Lei,[‡] Baoping Wang,[‡] Didier Pribat,[⊥] Gehan A. J. Amaratunga,[†] and William I. Milne[†,∥]

[†]Department of Engineering, Electrical Engineering Division, University of Cambridge, 9 JJ Thomson Avenue, CB3 0FA, Cambridge, United Kingdom, [‡]Display Research Centre, School of Electronic Science and Engineering, Southeast University, Nanjing 210096, People's Republic of China, [§]Department of Materials Science and Metallurgy, University of Cambridge, Pembroke Street, Cambridge, CB2 3QZ, United Kingdom, [⊥]Department of Energy Science, Sungkyunkwan University, Suwon, 440-746, Republic of Korea, and [∥]Department of Information Display, Kyung Hee University, Seoul 130-701, Republic of Korea. [#]Authors contributed equally.

ABSTRACT

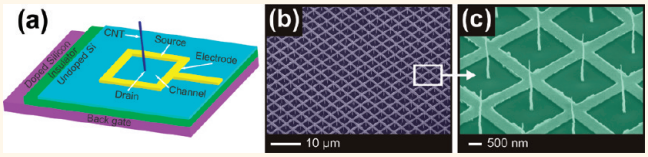

We present electronically controlled field emission characteristics of arrays of individually ballasted carbon nanotubes synthesized by plasma-enhanced chemical vapor deposition on silicon-on-insulator substrates. By adjusting the source−drain potential we have demonstrated the ability to controllable limit the emission current density by more than 1 order of magnitude. Dynamic control over both the turn-on electric field and field enhancement factor have been noted. A hot electron model is presented. The ballasted nanotubes are populated with hot electrons due to the highly crystalline Si channel and the high local electric field at the nanotube base. This positively shifts the Fermi level and results in a broad energy distribution about this mean, compared to the narrow spread, lower energy thermalized electron population in standard metallic emitters. The proposed vertically aligned carbon nanotube field-emitting electron source offers a viable platform for X-ray emitters and displays applications that require accurate and highly stable control over the emission characteristics.

KEYWORDS: carbon nanotubes · field emission · transistor · ballasted · hot electrons

Due to their high aspect ratio, small tip radius, excellent chemical stability, high thermal conductivity, and mechanical strength; carbon nanotubes (CNT)—one-dimensional carbon allotropes—have attracted much attention as field emission (FE) electron sources in flat panel displays,[1,2] environmental lighting,[3] parallel electron-beam lithography equipment,[4] X-ray sources,[5,6] and vacuum microwave amplifiers.[7,8] However, high emission currents, high uniformity, high stability, low driving field, and long lifetimes have yet to be demonstrated convincingly.

The emission current, given by the Fowler−Nordheim (FN) equation,[9] is strongly dependent on the field enhancement factor, which is a function of the local geometry of the emitting tip. The local electric field distribution can be detrimentally modified by nearby conducting structures.[10,11] If the emission current exceeds a well-defined maximum value (typically ∼20 μA),[12] which depends on the specific nanotube geometry, then irreversible structural modifications can occur, results in a runaway degradation process where increasingly large currents are emitted, which eventually destroys the tip.[13,14] To attain large emission currents, it is necessary to combine the currents from multiple (≥10 000) vertically aligned individual nanotubes in engineered arrays.[15,16] Such arrays must be bound to conducting substrates to minimize the substrate−nanotube interfacial resistance and to allow emitter biasing. Detrimental effects, such as electric field augmentation, are mitigated by employing high aspect ratio emitters,[17] while nearest neighbor electrostatic shielding,[12] induced by other nanotubes in the array, can be efficiently minimized by spacing the tips approximately twice their height from one another in regular patterns.[10] However, even small variations in the tip radii or emitter height result in considerable variation in the local electric field enhancement between tips. Consequently, in common cathode arrangements, each tip offers an unequal current contribution to the total emission current, causing the destruction of those dominating tips offering the largest current contributions. As a result, arrays of nanotube-based field emitters have been seldom employed as practical electron sources.

* Address correspondence to yz236@cam.ac.uk; lw@seu.edu.cn; mtc35@cam.ac.uk.

Received for review January 9, 2012 and accepted March 6, 2012.

Published online March 06, 2012
10.1021/nn300111t

© 2012 American Chemical Society

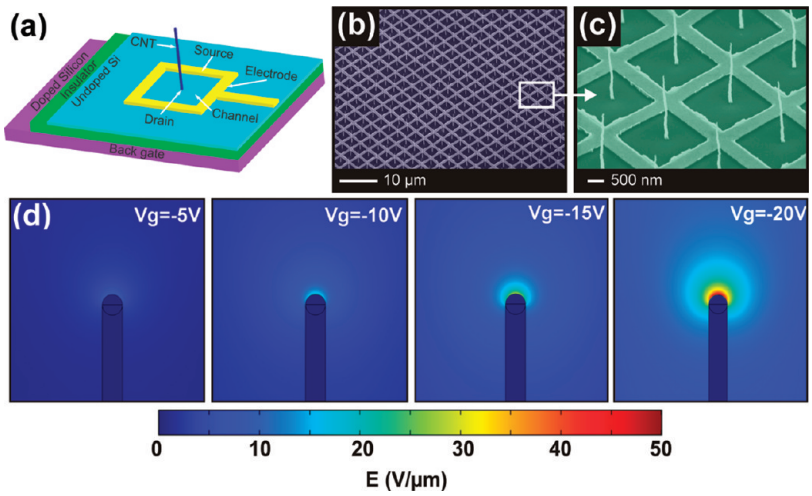

Figure 1. (a) Schematic of a single SOI-ballasted nanotube electron emitter showing the W circumferential source electrode surrounding the nanotube-drain electrode. (b) SEM micrographs of a fabricated triode ballasted nanotube electron emitter array consisting of 10^4 emitters each with an individual ballast. (c) High-magnification SEM micrograph of a few ballasted emitters. (d) *Ab initio* simulations of the local electric field as a function of the gate bias (V_g). Enhanced tip electric fields for (left to right) $V_g = -5, -10, -15,$ and -20 V.

Although some of the reported emitters have achieved very high emission currents,[18−21] their lifetimes are often poor. The integration of a ballast resistance in series with *each* nanotube emitter redistributes the individual current contributions by reducing the local electric field in proportion to the emission. Indeed, our previous work,[22] and others,[23,24] showed that ZnO NWs directly deposited onto nanotube arrays performed as efficient integrated ballast resistors.

In order to have a significant effect, the value of the ballast resistance must be comparable to the gradient of the I−V characteristic estimated from prior studies on field emission from nanotube arrays.[25] Large resistances are difficult to realize using metallic thin films, and the individual resistances require a variation proportional to the emitter aspect ratio.[26,27] Nevertheless, a ballast transistor architecture[28,29] integrated with each nanotube can facilitate very large resistances where the channel characteristics can be controlled in proportion to the emission current, provided a suitable feedback signal is accessible.

In the proposed structure, each emitter is connected in series to a single field effect transistor (FET) fabricated in silicon-on-insulator (SOI). As the emission current increases, in response to an increasing anode−cathode potential difference, the potential drop across the channel of the transistor also increases, tending to limit the rise in emission current by reducing the tip-to-anode potential difference. A schematic diagram of a single nanotube tip with an integrated ballast transistor is shown in Figure 1a. Electron micrographs of a typical fabricated device are given in Figure 1b, c. The channel resistance depends critically on the operating conditions of the transistor. The FET is formed from an undoped channel and a 200 nm thick thermally oxidized SiO_2 gate dielectric with asymmetric source and drain contacts. The source contact is a square metal mesh in direct contact with the Si, functioning as an abundant source of electrons when connected to the negatively biased power supply. The drain contact is formed at the nanotube/catalyst junction and has a contact area of $<10^{-14}$ m^2. This drain contact receives electrons and cannot source them in response to transport through the channel. As the electron current increases, the potential at the drain contact becomes positive and the gate−drain potential difference becomes increasingly negative, leading to a "pinch-off"-type current saturation in the field emission characteristics.

To better understand the function of the gate potential, *ab initio* simulations were performed on single transistor ballasted nanotubes, with dimensions as defined above, using COMSOL Multiphysics (v. 3.5a). The salient features of the simulation are shown in Figure 1d. The cathode was grounded, and the anode biased to 10 V, giving a global electric field of 2 V/μm. The gate electrode was set to -5, -10, -15, or -20 V to monitor the spatially evolving electric field. Equipotential energy contours around the nanotube tip are plotted in Figure 1d, showing the high degree of sensitivity of the emission on the gate bias. Simulations suggested that increasing the gate voltage to approximately 10 V effectively modified the local electric field by more than 50 times, thereby modulating the emission current driven by the anode−cathode potential difference.

The as-grown nanotubes had a mean length and diameter of 1.25 μm and 80 nm. The emitters were highly uniform, with a minor, $\pm$4.9% variation in length. Energy-dispersive X-ray measurements and

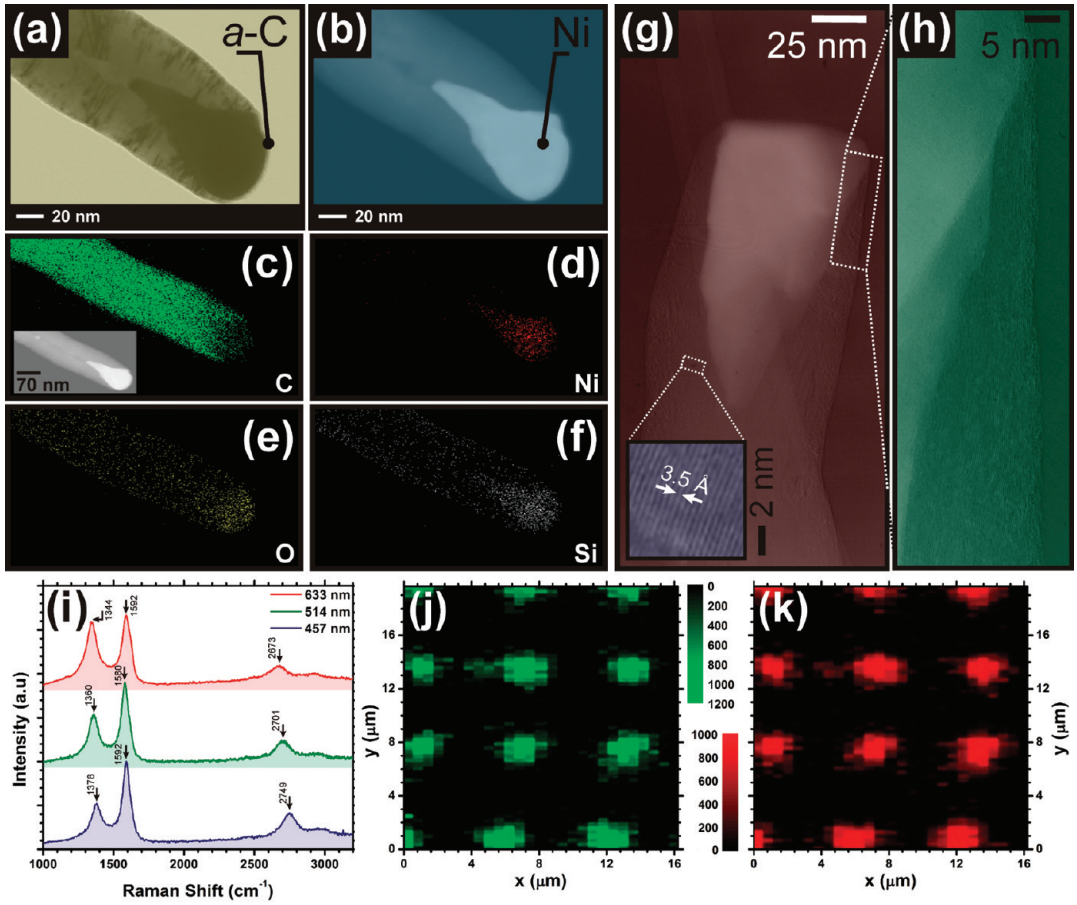

Figure 2. Emitter composition and crystallography. Bright field (a) and dark field (b) STEM micrographs (scale bar 20 nm) of a PE-CVD CNT electron emitter. (c–f) EDX maps showing (c) C, (d) Ni, (e) O, and (f) Si. Inset: Electron micrograph of the area under investigation (scale bar 50 nm). (g) TEM micrograph of a tip. Part of the lacey carbon support is seen in the background. Inset: HR-TEM micrograph showing the periodic graphitic lattice with an inter-shell spacing of 3.5 Å. (h) HR-TEM micrograph of the catalyst–sidewall interface. (i) 633, 514, and 457 nm Raman spectra of a typical emitter. The arrows depict (left to right) the D-, G-, and G′-peaks. (j) 16 × 20 μm ($\Delta_{x,y}$ = 300 nm) intensity maps of the (j) G-peak and (k) D-peak (532 nm, 2 mW), illustrating the highly uniform graphitization of a 6 μm pitch CNT array.

high-resolution transmission electron microscopy (HR-TEM) showed that the Ni catalyst resides at the emitter apex (Figure 2a–f) and that the tubes are bamboo-like in structure (Figure 2g, h). Figure 2i shows the 457, 514, and 633 nm Raman signatures of the emitters, showing characteristic features of plasma-enhanced chemical vapor deposition (PE-CVD) synthesized nanotubes.[30] Spatially resolved Raman maps of the defect-induced D-peak, defined as the C–C breathing modes of the 6-fold rings from K-point phonons of A_{1g} symmetry,[31] and the G-peak, the first-order scattering of the E_{2g} phonon at the Brillouin zone center,[32] illustrate the extremely high uniformity of the emitters, as presented in Figure 2j, k.

RESULTS AND DISCUSSION

Figure 3a shows the measured field-emitted current–electric field (I–E) curves at different gate voltages (0 to −20 V at −5 V increments). Figure 3b shows the corresponding FN plot where the data has been fitted to the Fowler–Nordheim equation, as defined by[33,34]

$$I = V^2\beta^2\left(\frac{A^*A}{\phi\delta^2}\right)\exp\left(\frac{-B\phi^{3/2}\delta}{\beta V}\right) \qquad (1.1)$$

where δ is the anode–cathode separation, A and B are the First and Second Fowler–Nordheim Constants, A^* is the effective emission area, Φ is the work function (4.8 eV) of the emitter, and β is the field enhancement factor which is proportional to the aspect ratio of the electron emitter. There are three particular regions of interest Figure 3a. The 0–6 V/μm shows the noise current prior to the application of the turn-on field, the 6–11 V/μm shows the pure field emission current (FN regime), and the >11 V/μm shows the transistor-limited emission current. In the FN regime, the I–E curves clearly evidence that the driving field is reduced when the gate voltage becomes increasingly negative. The negative gate voltage enhances the local electric field at the nanotube tips, as predicted by the earlier simulations.

The I–E curves show saturation attributed to the integrated transistor. At a fixed gate voltage (−20 V)

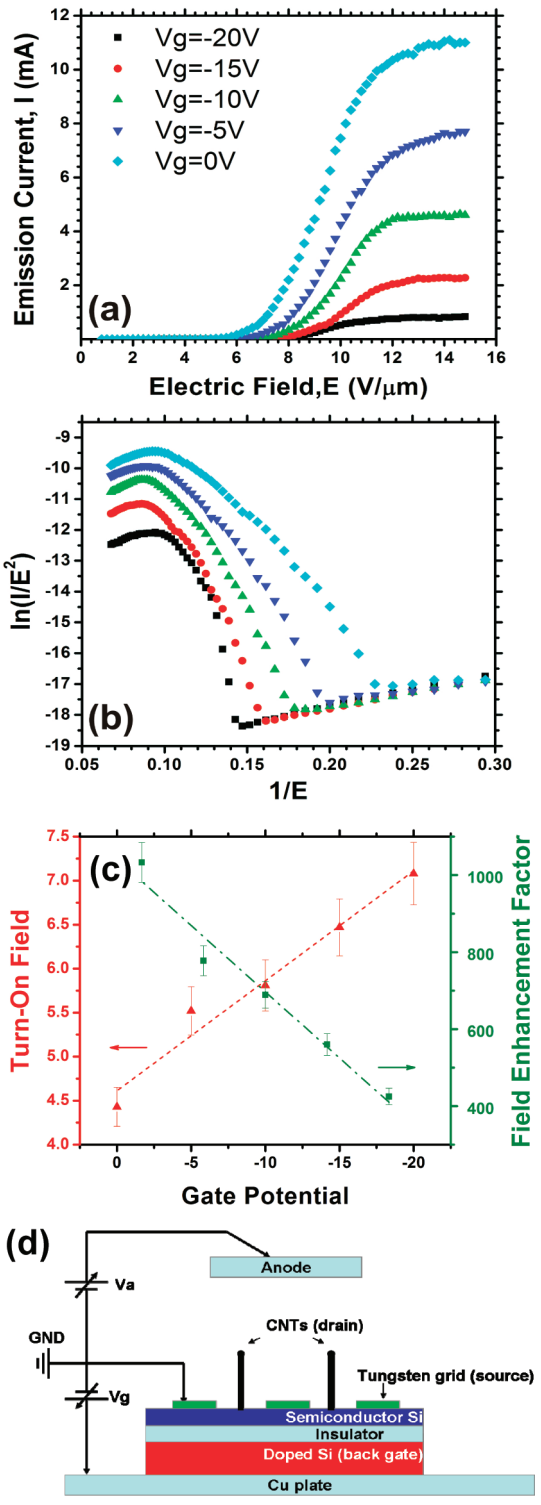

Figure 3. (a) Measured *I*−*V* curves at different gate voltage (V_g) and (b) the corresponding FN plot. (c) Gate potential dependence of the turn-on potential (defined as the field required to emit 1 μA) and the field enhancement factor. (d) Experimental triode setup.

the emission current saturated at 10 mA at an anode voltage of 3.5 kV (14 V/μm), corresponding to a current density of 10 A/cm^2. Assuming each nanotube tip operates at nominal emission, the emission current from a single tip was ~690 nA per emitter. According to our previous results,[12,35] a maximum emission current of approximately 20 μA can be obtained from PE-CVD synthesized nanotubes of this type. Evidently the estimated emission current is well within the safe tolerances and would suggest that the reported arrays can emit in excess of 100 mA.

The integrated intensity images (ZnO:Zn phosphor), measured at an extraction field of 1 V/μm and gate potentials of −5, −10, −15, and −20 V, are given in Figure 4. The full-width at half-maximum in each case is approximately 900 μm and is largely independent of the gate potential, suggesting that electrically ballasting the device does not degrade the focusability of the emitting array to any great degree.

The temporal emission characteristics are given in Figure 5. Figure 5a shows an accelerated lifetime test. The stability of the ballasted structure was greatly improved compared to previous works,[36,37] showing an extremely low emission current fluctuation of only ±0.68%, which is, to the best of the authors' knowledge, one of the lowest ever reported values. We attribute this to (i) the ballast structures redistributing the emission current from individual nanotube tips and protecting nanotubes from burning out and (ii) hot electrons in short channel semiconductor devices enhancing the field emission. We herein discuss the latter in more detail below. The transient response is shown in Figure 5b. Extremely fast on/off leading and trailing edges of <50 μs are noted.

Electrons accumulating at the drain become "hot" due to the large potential drop along the channel, as previously identified in *a*-C[38] and GaAs.[39] Hot electrons propagate through the nanotube and are readily emitted relative to their thermalized counterparts. In a conventional field emission system, the electron energy distribution is characterized by ambient temperature and defects along the length of the nanotube scatter the electrons being transmitted toward the tip, thereby ensuring their thermalization. Field emission is determined by the transmission probability of electrons from the Fermi sea in the tip through the triangular potential barrier into the vacuum.[9,40] The injection of hot electrons from the ballast transistor modifies the transport through the nanotube. These electrons are scattered much less effectively and arrive at the tip with sufficient excess momentum to significantly enhance the transmission.

The field enhancement factors decrease monotonically for increasingly negative gate potentials, while the turn-on field (defined as the field necessary to emit 1 μA) increases linearly with increasingly negative gate potentials, as shown in Figure 3c. Low gate potentials decrease the channel resistance and increase the energy of the transported electrons. This results in a corresponding increase in the injection depth across the Si/nanotube interface, resulting in reduced turn-on

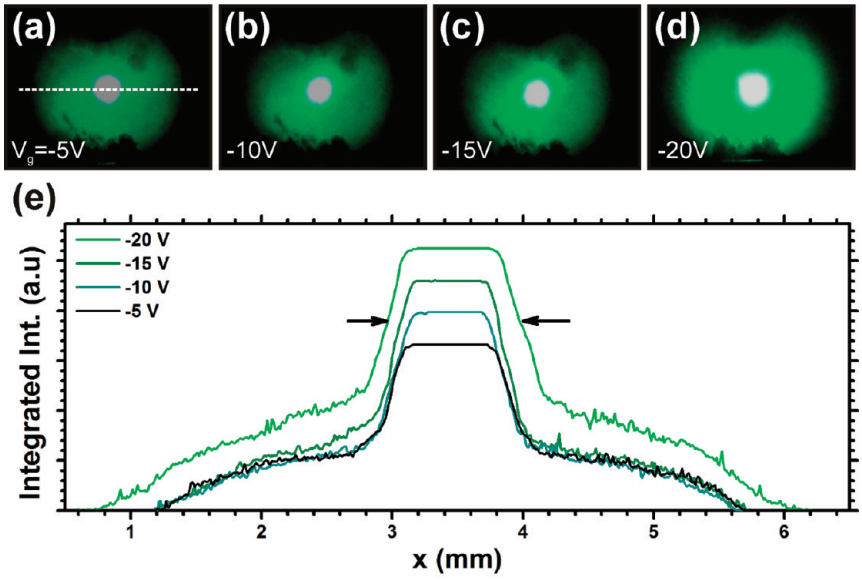

Figure 4. Integrated intensity maps (approximately 6 × 6 mm) at V_g = −5 V (a), −10 V (b), −15 V (c), and −20 V (d) for an extraction field of 1 V/μm.

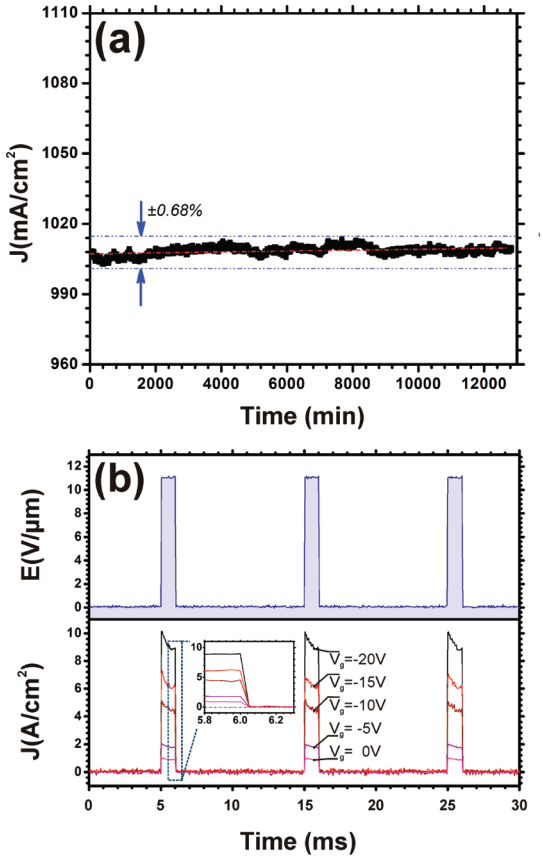

Figure 5. (a) Accelerated lifetime measurement (5 × 10^{-6} mbar) over 1.3 × 10^4 min showing an extremely small and stable ±0.68% variation at V_g = 0 V. (b) Transient response for fixed V_g = 0, −5, −10, −15, and −20 V and a 10% duty cycle with a 1 ms pulse width and an extraction field of 12 V/μm (top panel). Inset: Detail of a typical trailing edge.

fields as these hot electrons propagate further into the nanotube before thermalizing, and therefore a higher local electric field is observed. The enhanced transmission leads to an increase in the emission current compared to unballasted devices and possibly induces a deviation from conventional Fowler−Nordheim behavior. The increased transmission is most effective in the low-field (<6 V/μm) range, where the tip transmission is very low in conventional arrays. As the electric field increases, the tip transmission is correspondingly increased, such that the enhancement owing to the hot electrons is diminished.

Tip failure at high emission currents is due to heating of the emitter material, which induces increased atomic mobility and eventual sublimation.[41] Prior to sublimation, surface tension effects decrease the radius of curvature of the tip, thereby increasing the field enhancement factor. Heating may result from ohmic (I^2R) losses;[12] however this is unlikely in metallic or carbon-based emitters due to their comparatively low resistivity. Heating in field emission systems can also result from the Nottingham effect.[42] Electrons from well below the Fermi energy (cold electrons) contribute to the total emission, causing an increase in temperature. If a significant number of hot electrons are present, then this process is reversed and the tip is cooled.

CONCLUSIONS

We have demonstrated the fabrication and emission characteristics of individually integrated ballast transistors with carbon nanotube field emitters, which increase the current contribution of all the nanotube tips while preventing overemission and tip burn off, within regular nanotube arrays, particularly in the low-field region, due to hot electron effects. Simultaneous limiting of current in the high-field region, due to the intrinsic resistance of the channel, is also shown in

addition to electronic control over the emission current and field enhancement factor. The uniformity of the field emission current showed an extremely low fluctuation of only ±0.68%, which is one of the best ever reported stabilities to date. The emitters show rapid turn-on/off times of less than 50 μs and offer a viable platform for highly stable X-ray sources.

METHODS

Fabrication of the Ballasted Carbon Nanotube Arrays. Ballasted arrays were fabricated by casting poly(methylmethacrylate) (PMMA) onto a silicon-on-insulator substrate. A dot array was patterned by electron beam lithography (EBL). Ni (7 nm) catalyst and an ITO (20 nm) diffusion barrier were then deposited by magnetron sputtering, and residual PMMA and other organics were removed in repeated acetone baths. The W source electrodes were similarly defined and deposited by EBL and magnetron sputtering. The nanotubes were grown in a commercially available Black Magic PE-CVD system, the details of which are reported elsewhere.[7,43] Scanning electron micrographs of an as-fabricated ballasted emitter are given in Figure 1b, c. The W grids have a 2.5 μm × 2.5 μm pitch and a width of 0.5 μm. A single nanotube is located at the center of each square. The total emission area was 0.3 mm × 0.3 mm, formed from arrays containing 14 400 nanotubes.

Carbon Nanotube Analysis. Electron micrographs were generated using a Zeiss scanning electron microscope (SEM), a Hitachi S-5500 scanning transmission electron microscope (STEM) fitted with an Oxford Instruments mapping energy-dispersive X-ray (EDX) spectrometer, and a JEOL 400EX high-resolution transmission electron microscope (HR-TEM). Raman spectroscopic measurements were performed using a Renishaw InVia spectrometer operated at 457, 514, 532, and 633 nm with an incident power of 10 mW.

Field Emission Characterization. Ballasted arrays were loaded into a custom-built, ultrahigh-vacuum chamber evacuated to a base pressure of $<10^{-9}$ mbar. Samples were heated to 200 °C for 24 h to eliminate water vapor and possible adsorbates. The experimental setup for the field emission measurements is shown in Figure 3d. An interelectrode distance of 250 μm was defined using ceramic spacers. The metal grid (top electrode) was grounded. The anode was positively biased using a variable dc voltage supply (V_a). The emission current was measured using a Keithley 485 picoammeter. The gate voltage (V_g) was controlled by a secondary power supply.

Conflict of Interest: The authors declare no competing financial interest.

Acknowledgment. This work was supported by the European Commission through the AXIS project (Grant No. FP7-SME-1-2007) and the Scientific Research Foundation of the Graduate School of Southeast University, China (Grant No. YBJJ0926). M.T.C. thanks St Edmunds College Cambridge and the Isaac Newton Trust for their generous financial support. D.P. acknowledges support from the National Research Foundation of Korea and the Ministry of Education, Science and Technology (Grant No. R31-2008-000-10029-0). The authors thank the Cavendish Laboratory, Cambridge University, for the kind use of their Raman spectrometer facilities. The authors C.L., Y.Z., and M.T.C. contributed equally to this work.

REFERENCES AND NOTES

1. De Heer, W. A.; Châtelain, A.; Ugarte, D. A Carbon Nanotube Field-Emission Electron Source. *Science* **1995**, *270*, 1179–1180.
2. Dean, K. A. New Era—Nanotube Displays. *Nat. Photonics* **2007**, *1*, 273–275.
3. Baughman, R. H.; Zakhidov, A. A.; de Heer, W. A. Carbon Nanotubes—the Route toward Applications. *Science* **2002**, *297*, 787–792.
4. Wei, W.; Jiang, K.; Wei, Y.; Liu, P.; Liu, K.; Zhang, L.; Li, Q.; Fan, S. Lab6 Tip-Modified Multiwalled Carbon Nanotube as High Quality Field Emission Electron Source. *Appl. Phys. Lett.* **2006**, *89*, 1–3.
5. Liu, Z.; Yang, G.; Lee, Y. Z.; Bordelon, D.; Lu, J.; Zhou, O. Carbon Nanotube Based Microfocus Field Emission X-Ray Source for Microcomputed Tomography. *Appl. Phys. Lett.* **2006**, *89*, 1–3.
6. Zhang, J.; Yang, G.; Cheng, Y.; Gao, B.; Qiu, Q.; Lee, Y. Z.; Lu, J. P.; Zhou, O. Stationary Scanning X-Ray Source Based on Carbon Nanotube Field Emitters. *Appl. Phys. Lett.* **2005**, *86*, 1–3.
7. Teo, K. B. K.; Chhowalla, M.; Amaratunga, G. A. J.; Milne, W. I.; Pirio, G.; Legagneux, P.; Wyczisk, F.; Pribat, D.; Hasko, D. G. Field Emission from Dense, Sparse, and Patterned Arrays of Carbon Nanofibers. *Appl. Phys. Lett.* **2002**, *80*, 2011–2013.
8. Milne, W. I.; Teo, K. B. K.; Mann, M.; Bu, I. Y. Y.; Amaratunga, G. A. J.; De Jonge, N.; Allioux, M.; Oostveen, J. T.; Legagneux, P.; Minoux, E.; *et al.* Carbon Nanotubes as Electron Sources. *Phys. Status Solidi A* **2006**, *203*, 1058–1063.
9. Fowler, R. H.; Nordheim, L. Electron Emission in Intense Electric Fields. *Proc. R. Soc. London Ser. A* **1928**, *119*, 173–181.
10. Nilsson, L.; Groening, O.; Emmenegger, C.; Kuettel, O.; Schaller, E.; Schlapbach, L.; Kind, H.; Bonard, J. M.; Kern, K. Scanning Field Emission from Patterned Carbon Nanotube Films. *Appl. Phys. Lett.* **2000**, *76*, 2071–2073.
11. Groning, O.; Kuttel, O. M.; Emmenegger, C.; Groning, P.; Schlapbach, L. Field Emission Properties of Carbon Nanotubes. *J. Vac. Sci. Technol. B* **2000**, *18*, 665–678.
12. Milne, W. I.; Teo, K. B. K.; Amaratunga, G. A. J.; Legagneux, P.; Gangloff, L.; Schnell, J. P.; Semet, V.; Binh, V. T.; Groening, O. Carbon Nanotubes as Field Emission Sources. *J. Mater. Chem.* **2004**, *14*, 933–943.
13. Liang, X. H.; Deng, S. Z.; Xu, N. S.; Chen, J.; Huang, N. Y.; She, J. C. On Achieving Better Uniform Carbon Nanotube Field Emission by Electrical Treatment and the Underlying Mechanism. *Appl. Phys. Lett.* **2006**, *88*, 1–3.
14. She, J. C.; Xu, N. S.; Deng, S. Z.; Chen, J.; Bishop, H.; Huq, S. E.; Wang, L.; Zhong, D. Y.; Wang, E. G. Vacuum Breakdown of Carbon-Nanotube Field Emitters on a Silicon Tip. *Appl. Phys. Lett.* **2003**, *83*, 2671–2673.
15. Teo, K. B. K.; Lee, S. B.; Chhowalla, M.; Semet, V.; Binh, V. T.; Groening, O.; Castignolles, M.; Loiseau, A.; Pirio, G.; Legagneux, P., *et al.* In *Plasma Enhanced Chemical Vapour Deposition Carbon Nanotubes/Nanofibres—How Uniform Do They Grow?*, 3rd International Conference on Trends in Nanotechnology, Santiago Composte, Spain, Sept 9—13, 2002; Iop Publishing Ltd: Santiago Composte, Spain, **2002**; pp 204—211.
16. Teo, K. B. K.; Chhowalla, M.; Amaratunga, G. A. J.; Milne, W. I.; Legagneux, P.; Pirio, G.; Gangloff, L.; Pribat, D.; Semet, V.; Binh, V. T.; *et al.* Fabrication and Electrical Characteristics of Carbon Nanotube-Based Microcathodes for Use in a Parallel Electron-Beam Lithography System. *J. Vac. Sci. Technol. B* **2003**, *21*, 693–697.
17. Bonard, J. M.; Salvetat, J. P.; Stockli, T.; de Heer, W. A.; Forro, L.; Chatelain, A. Field Emission from Single-Wall Carbon Nanotube Films. *Appl. Phys. Lett.* **1998**, *73*, 918–920.
18. Zhu, W.; Bower, C.; Zhou, O.; Kochanski, G.; Jin, S. Large Current Density from Carbon Nanotube Field Emitters. *Appl. Phys. Lett.* **1999**, *75*, 873–875.
19. Yan, C.; Patel, S.; Yagu, Y.; Shaw, D. T.; Liping, G. Field Emission from Aligned High-Density Graphitic Nanofibers. *Appl. Phys. Lett.* **1998**, *73*, 2119–2121.

20. Lee, C. J.; Park, J.; Kang, S. Y.; Lee, J. H. Growth and Field Electron Emission of Vertically Aligned Multiwalled Carbon Nanotubes. *Chem. Phys. Lett.* **2000**, *326*, 175–180.
21. Rao, A. M.; Jacques, D.; Haddon, R. C.; Zhu, W.; Bower, C.; Jin, S. In Situ-Grown Carbon Nanotube Array with Excellent Field Emission Characteristics. *Appl. Phys. Lett.* **2000**, *76*, 3813–3815.
22. Li, C.; Zhang, Y.; Mann, M.; Hiralal, P.; Unalan, H. E.; Lei, W.; Wang, B. P.; Chu, D. P.; Pribat, D.; Amaratunga, G. A. J.; *et al*. Stable, Self-Ballasting Field Emission from Zinc Oxide Nanowires Grown on an Array of Vertically Aligned Carbon Nanofibers. *Appl. Phys. Lett.* **2010**, *96*, 143114–143117.
23. Yan, X.; Tay, B.-K.; Miele, P. Field Emission from Ordered Carbon Nanotube-Zno Heterojunction Arrays. *Carbon* **2008**, *46*, 753–758.
24. Jo, S. H.; Banerjee, D.; Ren, Z. F. Field Emission of Zinc Oxide Nanowires Grown on Carbon Cloth. *Appl. Phys. Lett.* **2004**, *85*, 1407–1409.
25. Cui, J. B.; Teo, K. B. K.; Tsai, J. T. H.; Robertson, J.; Milne, W. I. The Role of Dc Current Limitations in Fowler-Nordheim Electron Emission from Carbon Films. *Appl. Phys. Lett.* **2000**, *77*, 1831–1833.
26. Jong Duk, L.; Il Hwan, K.; Chang Woo, O. Implementation of Fed with Mosfet-Controlled Fea. *Eleventh International Vacuum Microelectronics Conference* **; 1998.**
27. Kymissis, I.; Akinwande, A. I. Organic Tft Controlled Organic Field Emitter. *Technical Digest of the 16th International Vacuum Microelectronics Conference* **2003**; pp 37−38.
28. Velasquez-Garcia, L. F.; Guerrera, S. A.; Ying, N.; Akinwande, A. I. Uniform High-Current Cathodes Using Massive Arrays of Si Field Emitters Individually Controlled by Vertical Si Ungated Fets; Part 1: Device Design and Simulation. *IEEE Trans. Electron Devices* **2011**, *58*, 1775–1782.
29. Velasquez-Garcia, L. F.; Adeoti, B.; Niu, Y.; Akinwande, A. I. Uniform High Current Filed Emission of Electrons from Si and Cnf Feas Individually Controlled by Si Pillar Ungated Fets. *IEDM. Washington 2007/IEEE International*; **2007**; pp 599−602.
30. Chhowalla, M.; Teo, K. B. K.; Ducati, C.; Rupesinghe, N. L.; Amaratunga, G. A. J.; Ferrari, A. C.; Roy, D.; Robertson, J.; Milne, W. I. Growth Process Conditions of Vertically Aligned Carbon Nanotubes Using Plasma Enhanced Chemical Vapor Deposition. *J. Appl. Phys.* **2001**, *90*, 5308–5317.
31. Ferrari, A. C. Raman Spectroscopy of Graphene and Graphite: Disorder, Electron-Phonon Coupling, Doping and Nonadiabatic Effects. *Solid State Commun.* **2007**, *143*, 47–57.
32. Ferrari, A. C.; Robertson, J. Interpretation of Raman Spectra of Disordered and Amorphous Carbon. *Phys. Rev. B* **2000**, *61*, 14095–14107.
33. Baker, F. S.; Williams, J.; Osborn, A. R. Field-Emission from Carbon Fibers−New Electron Source. *Nature* **1972**, *239*, 96–97.
34. Lee, M. J. G. Field-Emission of Hot-Electrons from Tungsten. *Phys. Rev. Lett.* **1973**, *30*, 1193–1196.
35. Milne, W. I.; Teo, K. B. K.; Chhowalla, M.; Amaratunga, G. A. J.; Lee, S. B.; Hasko, D. G.; Ahmed, H.; Groening, O.; Legagneux, P.; Gangloff, L.; *et al*. Electrical and Field Emission Investigation of Individual Carbon Nanotubes from Plasma Enhanced Chemical Vapour Deposition. *Diamond Relat. Mater.* **2003**, *12*, 422–428.
36. Nakamoto, M.; Moon, J.; Shiratori, K. Low Work Function Nanometer-Order Controlled Transfer Mold Field-Emitter Arrays. *J. Vac. Sci. Technol. B* **2010**, *28*, C2B1–C2B4.
37. Tseng, H. Y.; Wang, Y. W.; Chen, C. M.; Huang, C. Y.; Sheu, S. S.; Lin, W. Y.; Chen, Y. H.; Lin, M. H.; Lee, C. T. A 4-Inch Qvga Amcnt-Fed Driven by High Voltage Ltps-Tfts. *Proc. Int. Disp. Workshops* **2004**, *11*, 1171–1174.
38. Forrest, R. D.; Burden, A. P.; Silva, S. R. P.; Cheah, L. K.; Shi, X. A Study of Electron Field Emission as a Function of Film Thickness from Amorphous Carbon Films. *Appl. Phys. Lett.* **1998**, *73*, 3784–3786.
39. Fitting, H. J.; Hingst, T.; Schreiber, E.; Geib, E. Vacuum Emission of Hot and Ballistic Electrons from Gaas. *J. Vac. Sci. Technol. B* **1996**, *14*, 2087–2089.
40. Gomer, R. Field Emission and Field Ionization. In *Harvard Monographs in Applied Sciences*; Oxford University Press: London, 1961; Vol. 9, p 195.
41. Wei, Y.; Xie, C.; Dean, K. A.; Coll, B. F. Stability of Carbon Nanotubes under Electric Field Studied by Scanning Electron Microscopy. *Appl. Phys. Lett.* **2001**, *79*, 4527–4529.
42. Paulini, J.; Klein, T.; Simon, G. Thermo-Field Emission and the Nottingham Effect. *J. Phys. D* **1993**, *26*, 1310–1315.
43. Teo, K. B. K.; Hash, D. B.; Lacerda, R. G.; Rupesinghe, N. L.; Bell, M. S.; Dalal, S. H.; Bose, D.; Govindan, T. R.; Cruden, B. A.; Chhowalla, M.; *et al*. The Significance of Plasma Heating in Carbon Nanotube and Nanofiber Growth. *Nano Lett.* **2004**, *4*, 921–926.